

Fabrication of LiOH-metal organic framework derived hierarchical porous host carbon matrix composites for seasonal thermochemical energy storage

Xiangyu Yang^{1,3}, Shijie Li², Jianguo Zhao^{1,2} (✉), Hongyu Huang³ (✉), and Lisheng Deng⁴

¹ School of Materials Science and Engineering, Taiyuan University of Technology, Taiyuan 030024, China

² Institute of Carbon Materials Science, Shanxi Datong University, Datong 037009, China

³ Key Laboratory of Renewable Energy, Guangdong Provincial Key Laboratory of New and Renewable Energy Research and Development, Guangzhou Institute of Energy Conversion, Chinese Academy of Sciences, Guangzhou 510640, China

⁴ Guangdong Intelligent Filling Technology Limited Company, Foshan 528137, China

© Tsinghua University Press 2022

Received: 16 February 2022 / Revised: 7 April 2022 / Accepted: 9 April 2022

ABSTRACT

By virtue of its long lifespan and outstanding storage intensity with near-zero heat loss, salt hydrate thermochemical energy storage (TES) materials provide a feasible option for the effective use of renewable energy and overcoming its unsynchronized supply and demand. Here, an activated porous carbon originating from the zeolite imidazolate framework (ZHCM) is fabricated and served as the carbon matrix for the LiOH TES material. The as-synthesized Li/ZHCM2-40 not only has excellent storage intensity (maximum 2414.2 kJ·kg⁻¹) with low charging temperature, but also shows great hydration properties stemming from the ultrahigh surface area and hierarchical porous structure of ZHCM2. Besides, this composite material exhibits superior thermal conductivity, while its storage intensity is only attenuated by 10.2% after 15 times of consecutive charge–discharge process, revealing its outstanding cycle stability. And the numerical simulation results also demonstrate its superior heat transfer performance. The developed LiOH TES composite may afford a new avenue for efficient low-grade thermochemical energy storage and liberate the possibility of further exploration of metal organic frameworks derived porous carbon matrix in the future.

KEYWORDS

LiOH TES composite, ZIF-8 derived porous carbon, low-grade thermochemical energy storage, cycle stability

1 Introduction

With the accelerated consumption of energy brought by the high-quality development of the economy, as well as the environmental pollution caused by energy consumption, the energy crisis has become one of the central issues of global research [1, 2]. Currently, there are two main ways to alleviate the energy crisis: first, vigorously develop and utilize renewable energy to reduce dependence on primary energy; second, change the way of energy utilization, explore new technologies, and improve energy utilization efficiency, such as the recycling of industrial waste heat resources [3]. However, most renewable energy is greatly affected by the environment, and its shortcomings such as time discontinuity, spatial difference, and intensity instability have greatly restricted its large-scale application [4]. Besides, the fact that a great deal of industrial waste heat arising from traditional high-energy-consuming industries cannot be recycled is also an urgent energy waste problem that needs to be solved [5, 6]. Therefore, the development of energy storage systems that could ameliorate energy efficiency and solve the imbalance in energy distribution has become a challenge but an imperative issue that needs to be solved [7].

Recently, metal-organic frameworks (MOFs) have exhibited diverse implementation prospects in the areas of separation and

energy storage by virtue of its diverse structure, excellent specific surface area (SSA), favorable porosity and tailorable porous structure [8–10]. However, MOFs are relatively fragile in the face of heat and humidity, which greatly inhibits their practical implementation potential [11]. In this context, the idea of pyrolyzing the MOF into porous carbon materials provides a feasible strategy to tackle this problem and the resulting carbon materials have been implemented in various areas [12, 13]. This kind of carbon material combines the outstanding SSA, porosity and unique morphology of MOF, and the excellent heat transfer ability of the carbon material while minimizing the shortcomings of both materials, which makes it a rising star in the family of porous materials [14, 15]. On the other hand, most MOF-derived porous carbon materials are usually overwhelmed by micropores, which is unfavorable for the uniform diffusion of particles and mass transfer [16]. Inspired by the fabricated approach of activated carbon, applying the reliable chemical activation strategy that has been popular in traditional carbon materials to expand porosity to emerging carbon materials originated from MOFs may be a feasible solution to the above dilemma. Therefore, in order to further exert the superiorities of this porous carbon material as a host matrix, it is imperative to optimize its pore structure by selecting appropriate activation conditions and procedures [17].

Address correspondence to Jianguo Zhao, staket@foxmail.com; Hongyu Huang, huanghy@ms.giec.ac.cn

Surprisingly, compared to its fulfillment in other fields, MOF-derived porous carbon materials are relatively less active in the area of heat storage, especially no studies about the implantation of carbon matrix originated from MOFs in thermochemical energy storage (TES) have hitherto been published, indicating that the implementation scope of this material still has a lot of room for expansion.

Noticeably, the heat storage system that could overcome the incompatibility of time and space and reduce peak demand, as well as effectively storage of renewable energy, has gained credibility as a promising and feasible energy storage technology [18–20]. Particularly, the TES system with the merits of large heat storage capacity, almost zero heat loss, and long storage life span, which highlights its huge practical application potential [21, 22]. Among many TES systems, salt hydrate-based TES materials have become the limelight of thermal energy storage research ascribed to the non-toxicity and easy availability of raw material water and environmental friendliness as well as simple reaction mechanism [23, 24]. Nevertheless, the charging temperature of the majority of hydrated salt TES materials is higher than the actual temperature of industrial waste heat and solar thermal energy, which creates a vacancy in the utilization of low temperature thermal energy and greatly hinders its wide-ranging practical commercial popularization and application [25, 26]. Under such circumstances, the emergence of LiOH with the strengths of relatively low charging temperature and outstanding storage intensity put forward the research directions for making full use of low-grade energy such as solar thermal energy as well as underutilized waste heat [27, 28]. In addition, it is also equipped with the advantages of a simple reaction mechanism and no side reactions, which also eliminates considerable obstacles for the application and promotion of actual reactors in the future [29]. Despite great progress that has been made, pure lithium hydroxide still cannot overcome the inherent problems of poor thermal conductivity, agglomeration and swelling, poor hydration performance, and serious cycle attenuation of salt hydrates, which not only hinders its heat and mass transfer but also is a huge obstacle to its practical application [30]. Hence, it is remaining an intractable problem to develop a LiOH TES material with remarkable hydration performance and thermal conductivity, high heat storage density as well as outstanding cycle stability for

effective and seasonal low-grade heat source storage and efficient utilization.

In this work, we present the fabrication of an activated porous carbon (ZHCM) through pyrolysis of the zeolite imidazolate framework and the synthesis of LiOH TES composites using it as the host carbon matrix. Attributing to the ultrahigh SSA and desirable porosity of ZHCM2, Li/ZHCM2 shows great storage intensity and prominent hydration ability. In addition, the storage intensity of Li/ZHCM2 not only has no significant attenuation after 15 charge–discharge processes, but is also equipped with a significantly enhanced thermal conductivity, suggesting its eminent cycle stability and heat transfer performance as well as huge development value for domestic heating, as displayed in Fig. 1.

2 Experimental

2.1 Synthesis of ZIF-8 derived host carbon matrix

The preparation process of ZIF-8 derived host carbon matrix is as follows: typically, $\text{Zn}(\text{CH}_3\text{COO})_2 \cdot 2\text{H}_2\text{O}$ (4.39 g) and 2-methylimidazole (13.14 g) were respectively dissolved in 80 mL of deionized water, and then the two solutions were mixed and stirred for 15 min and then kept at 30 °C for 36 h. And ZIF-8 was obtained after washing the precipitate with methanol several times and drying at 60 °C for 12 h. Then the obtained ZIF-8 powder was heated to 800 °C at a heating rate of 5 °C·min⁻¹ and kept for 3 h under Ar atmosphere. After the carbonization was completed and cooled to 30 °C, the resulting black powder was immersed in HCl (2 M) for 18 h. Then the crude product was filtered and washed with deionized water several times until it was neutral, and the porous carbon prepared by direct carbonization of ZIF-8 was obtained after drying in vacuum at 80 °C for 12 h, named as ZPC.

Then 200 mg of ZPC was uniformly dispersed in an aqueous solution containing 400 mg of potassium hydroxide. After the water was completely removed, the resulting mixture was activated at 800 °C with a heating rate of 5 °C·min⁻¹ and kept for 1.5 h under Ar atmosphere. After cooling to 30 °C, the obtained black powder was immersed in HCl (1 M) for 2 h, and the crude product was filtered and washed with deionized water until it was neutral, and finally the ZIF-8 derived host carbon matrix was obtained after dried in vacuum at 80 °C for 12 h, named as

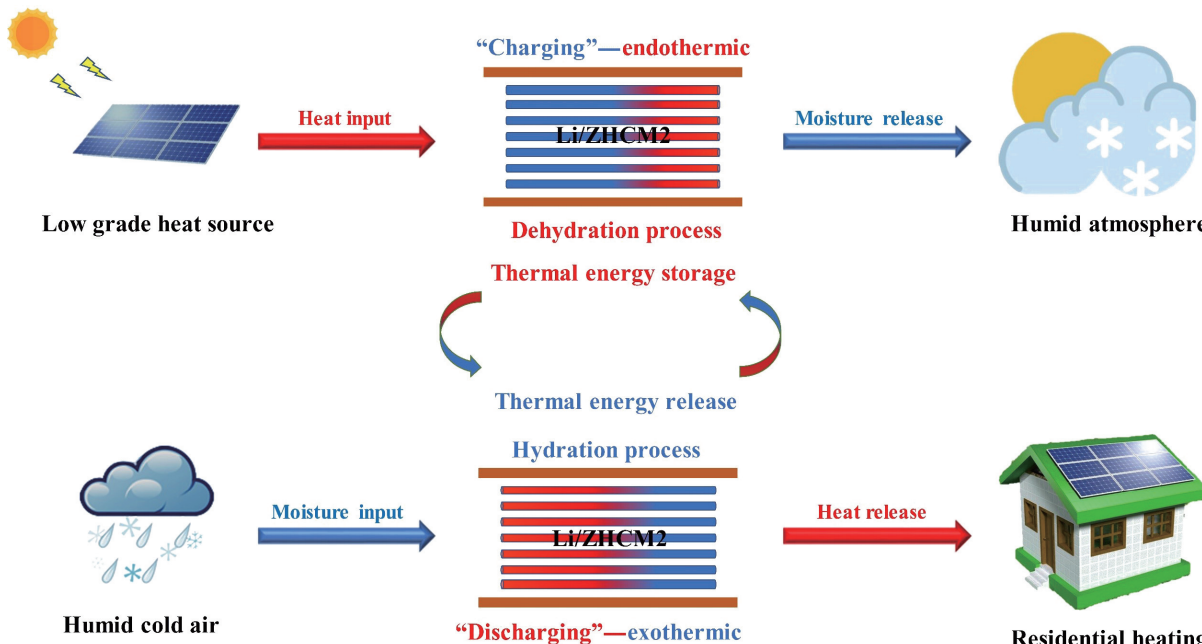


Figure 1 Diagrammatic sketch of the Li/ZHCM2 composite for renewables storage and transformation.

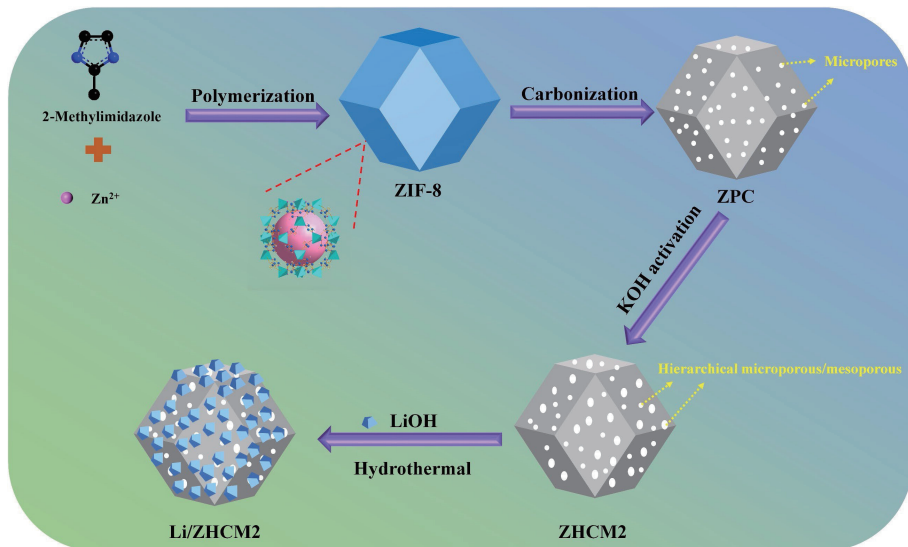


Figure 2 Preparation route of ZIF-8, ZPC, ZHCM2 and Li/ZHCM2 composites.

ZHCM2. For comparison, ZHCM1 and ZHCM3 were synthesized through similar steps except that the mass ratio of ZPC to KOH was changed to 1:1 and 1:3, respectively.

2.2 Preparation of LiOH-TES composites

The prepared ZHCM2 powder (50 mg) was added to 25 mL of deionized water with lithium hydroxide and stirred at 30 °C for 60 min. Then the mixture was placed in a Teflon autoclave and kept at 140 °C for 12 h. After cooling down to 30 °C, the resulting solution was dried at 120 °C for 4 h to obtain a completely dehydrated target LiOH-TES composite. The target products with different lithium hydroxide quantities (20 wt.%, 30 wt.%, 40 wt.%, and 50 wt.%) were named as Li/ZHCM2-20, Li/ZHCM2-30, Li/ZHCM2-40, and Li/ZHCM2-50, respectively, as displayed in Fig. 2. For comparison, Li/ZPC-40, Li/ZHCM1-40, and Li/ZHCM3-40 were prepared by similar steps, except that the ZIF-8 derived host carbon matrix was changed to ZPC, ZHCM1, and ZHCM3, respectively. Reagents, characterization section and heat transfer numerical simulation description are displayed in the Electronic Supplementary Material (ESM).

3 Results and discussion

3.1 Characterization of the host carbon matrix

The morphologies of ZIF-8, ZPC, ZHCM, pure LiOH, and Li/ZHCM2 composite were observed by scanning electron microscopy (SEM). As shown in Fig. 3(a), ZIF-8 presents the classic dodecahedron configuration accompanied by a flat surface. It can be seen from Fig. 3(b) that the ZPC prepared by direct carbonization at 800 °C maintains the primitive structural form and great porosity of ZIF-8 with an enhanced surface roughness level and a slightly decreased structure. In order to accomplish the goal of upgrading the SSA and enriching the pore architecture, ZPC was activated with KOH by utilizing its abundant defects and active sites. As shown in Fig. 3(c) and Fig. S1(a) in the ESM, although the morphology of ZHCM1 as well as ZHCM2 has not changed strikingly after the intense activation procedure, its surface has become even rougher than that of ZPC, which may be owing to the etching reaction between the carbon skeleton and KOH [31]. It can be speculated that the obtained ZHCM2 with larger SSA and optimized porosity as the host carbon matrix is obviously conducive to the uniform diffusion and mass transfer of salt hydrate [32]. Noticeably, when the activation ratio continues to increase to 1:3, the resulting ZHCM3 loses the structural

integrity of the precursor and is transformed into an irregular block with visible pores, which may be ascribed to the over-activation resulting from the excessive proportion of KOH, as displayed in Fig. S1(b) in the ESM [32]. This obvious morphological change may have a counterproductive effect on structural optimization with a clear purpose, and ultimately manifests itself as a weakening of the potential of ZHCM3 as a host carbon matrix [33]. Additionally, Fig. 3(d) shows that before being compounded with ZHCM2, the stature of pure lithium hydroxide is bloated with obvious agglutination, resulting in its insufficient hydration with water molecules. On the other hand, Fig. 3(e) shows that lithium hydroxide particles with smaller particle sizes are uniformly dispersed and anchored in ZHCM2, and the agglomeration phenomenon is also significantly alleviated, which not only can effectively upgrade the hydration ability of the composite, but also could make a greater contribution to the improvement of storage capacity.

The chemical structures of ZIF-8, ZPC, and ZHCMs as well as Li/ZHCM2-x composites were demonstrated by X-ray diffraction (XRD). Figure 4(a) demonstrates that the synthesized ZIF-8 exhibits the same zeolite-like structure as reported in the literature with sharp peaks, manifesting the successful preparation of ZIF-8 crystals with high crystallinity [34]. When ZIF-8 is carbonized at 800 °C, the broad peaks near 25° and 45°, which represent the peaks of amorphous as well as graphite carbon respectively, replace the disappearing characteristic peaks of ZIF-8, indicating that ZIF-8 has been fully pyrolyzed into porous carbon material [35]. It is worth noting that after ZPC is activated by KOH, the intensities of a series of ZHCM peaks at 25° and 45° decrease and the peaks also become broader compared with ZPC, indicating the highly defective and porous structure of ZHCM [17]. To achieve the purpose of acquiring a quantifiable assessment of the degree of defects of a series of different host carbon matrices, the empirical parameter (*R*) was obtained in the light of the ratio of the intensity of amorphous carbon peak to the background intensity [36]. And the *R* value is a well-established index that is proportional to the defect state of carbon materials [37]. Obviously, all ZHCMs present a smaller *R* value in comparison to ZPC, among which ZHCM3 exhibits the smallest *R* value of 1.16, manifesting that the defect degree of the carbon matrix has a strong positive correlation to the KOH dosage. Moreover, the Raman test was performed to further investigate the defect magnitude of different carbonaceous materials. Generally, the D band at 1,340 cm⁻¹ stands for amorphous carbon, while the G band at 1,580 cm⁻¹ stands for graphitized carbon, and the ratio of the two (*I*_D/*I*_G) could

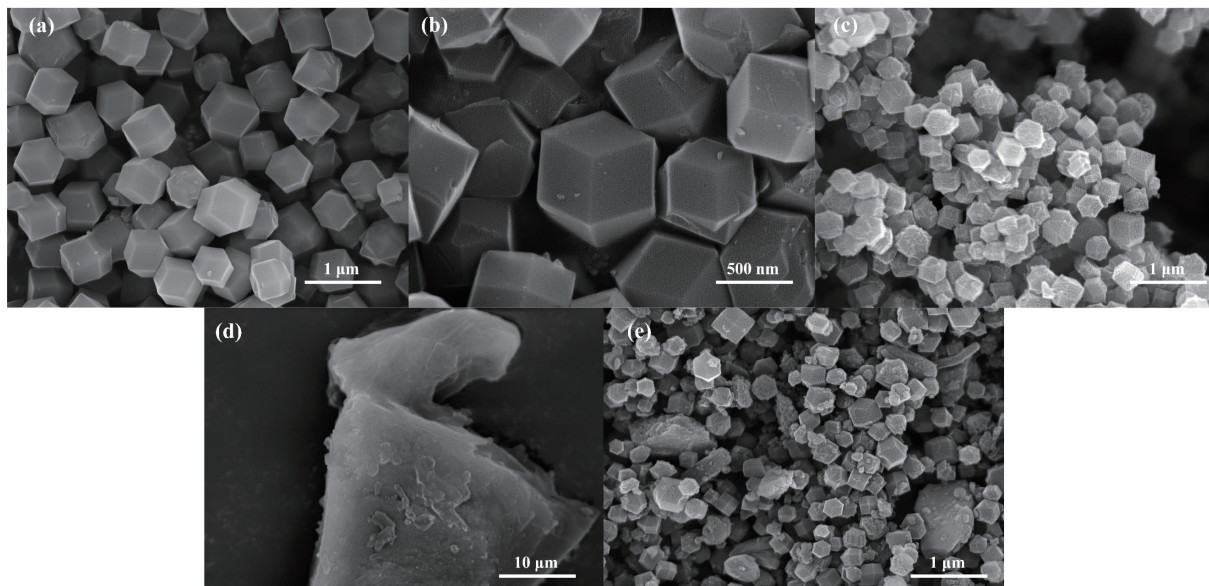


Figure 3 SEM pictures of (a) ZIF-8 crystal, (b) ZPC, (c) ZHCM2, (d) pure lithium hydroxide, and (e) Li/ZHCM2-40.

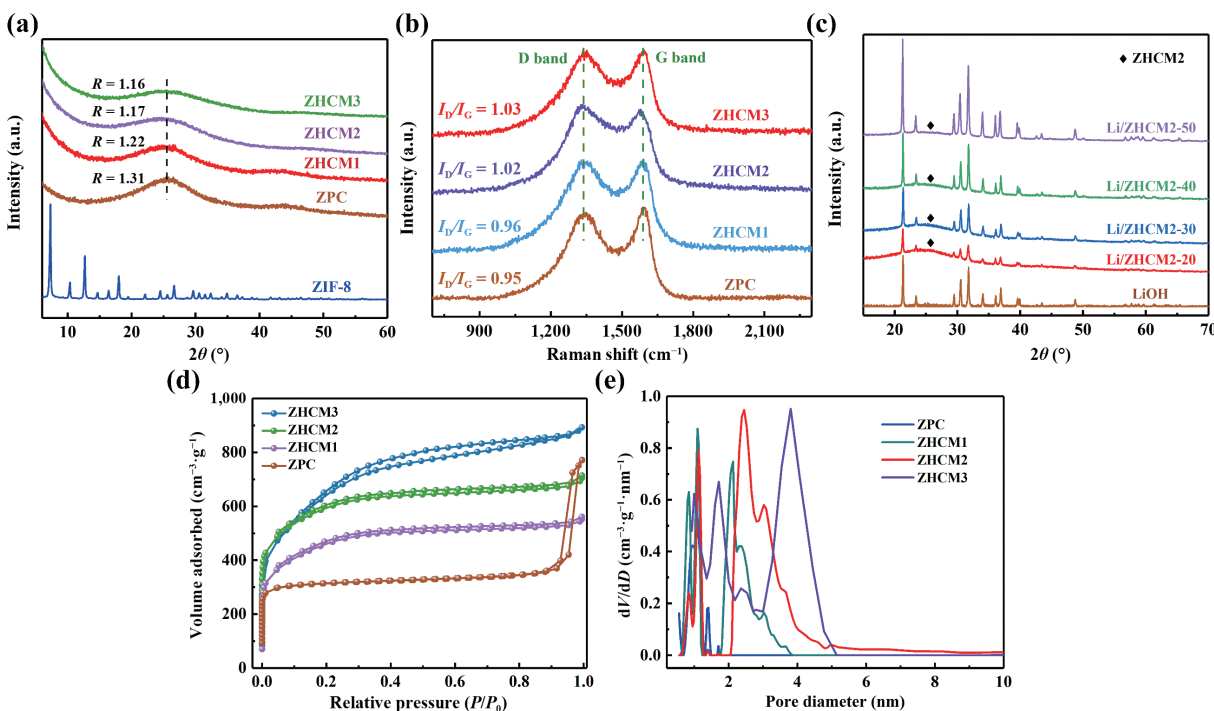


Figure 4 (a) XRD patterns of ZIF-8, ZPC, as well as ZHCMx with various KOH activation ratios. (b) Raman spectra of ZPC as well as ZHCMx with various KOH activation ratios. (c) XRD patterns of LiOH and Li/ZHCM2-20, Li/ZHCM2-30, Li/ZHCM2-40, and Li/ZHCM2-50. (d) N₂ adsorption-desorption isotherms and (e) pore size distribution of ZPC, ZHCM1, and ZHCM2 as well as ZHCM3.

demonstrate the defect magnitude of the carbon matrix [38]. It can be seen from Fig. 4(b) that all ZHCMs display higher I_D/I_G values in comparison to ZPC, proving the role of KOH in the optimization of the textural architecture of the host matrix. On the other hand, ZHCM2 exhibits a high I_D/I_G value of 1.02 while still maintaining the valuable original structure of the precursor intact, which indicates that it is equipped with more defects and a higher degree of disorder. This property of ZHCM2 makes it more favorable to the uniform scatter of LiOH and the corresponding upgradation in mass transfer performance, which also makes it the best choice as the host carbon matrix of LiOH TES composites. In addition, Fig. 4(c) shows that all Li/ZHCM2-x composites are not only equipped with the characteristic diffraction peak of LiOH, but also exhibit the amorphous carbon diffraction peak attributed to ZHCM2 at 26°, which indicates that LiOH particles and ZHCM2 have been successfully composited.

The textural parameters of ZPC and ZHCM-x with various KOH activation ratios were evaluated by N₂ adsorption-desorption test. Figure 4(d) shows that compared with the ZPC exhibiting a typical type I isotherm with a conspicuous precipitous raise at the low relative pressures, the adsorption-desorption curve of ZHCMx accompanied by a large hysteresis loop at the high relatively pressure shows a typical type IV isotherm, which not only indicates the fact that micropores hold a leading status in ZPC and both micropores as well as mesopores exist in ZHCMx, but also shows that the pore structure of ZPC has changed significantly after KOH activation [39]. The structural transformation of ZHCM is accompanied by an increase in SSA while diversifying its porosity structure with abundant mesopores and micropores, which is a vital guarantee for the good scatter of nano lithium hydroxide and the diffusion of water molecules. Strikingly, different from ZHCM1 and ZHCM2

with similar adsorption isotherms, the isotherm of ZHCM3 presents a more evident hysteresis loop at the relative pressure of $P/P_0 = 0.15\text{--}0.8$, which not only indicates the larger mesopores proportion in ZHCM3 but also indirectly verifies the texture change of ZHCM3 mainly caused by the morphology transition [40]. Those findings are also confirmed by the pore size distribution. From Fig. 4(e), it can be clearly observed that in sharp contrast to the ZPC with only micropores, ZHCM reveals its prominent micropore/mesoporous structure, which further certifies the active influence of KOH on the diversification of the porosity of the host matrix. Moreover, the proportion of mesopores in ZHCM also increases with the increase in the proportion of KOH activation, which is consistent with the findings of XRD and Raman. The corresponding textural parameters of all test materials could be found in Table S1 in the ESM. It is obvious that the SSA and pore volume of ZHCMs have exceedingly improved compared with ZPC due to KOH activation, which makes it more beneficial to the even scatter of salt hydrate. On the other hand, ZHCM2, which exhibits an ultrahigh SSA ($2371.2 \text{ m}^2\cdot\text{g}^{-1}$) with hierarchical microporous/mesoporous structure and a great pore volume of $1.96 \text{ cm}^3\cdot\text{g}^{-1}$, not only facilitates the uniform scatter of lithium hydroxide accompanied by a smaller size, but also assuages the serious agglutination of lithium hydroxide, making it a competitive option as the carbon matrix of LiOH TES composite materials.

3.2 Hydration performance

In terms of chemical heat storage based on salt hydrate, the hydration performance of TES materials is one of the crucial parameters that affect the actual heat storage properties. Hence, in order to screen out the best carbon matrix, the hydration rates and water sorption abilities of a series of LiOH TES composites with different carbon matrices under various conditions were investigated. As shown in Fig. 5(a), the water absorption of all composite materials increases with the passage of time and reaches an equilibrium state after a certain period of time, but the hydration rate between the samples exhibits a significant difference, in which Li/ZHCM2-40 shows the optimal hydration rate as well as water absorption of $0.49 \text{ g}\cdot\text{g}^{-1}$. Strikingly, the hydration rate between the four samples is positively correlated with the SSA and the degree of the defects as well as the structural integrity of the host carbon matrix according to Brunauer–Emmett–Teller (BET) and Raman results, which shows that there is an inseparable relationship between the microstructure of the carbon matrix of the material and the hydration rate. Besides, the investigation of the equilibrium water absorption capacity of each composite under various relative

humidity (RH) was also conducted. It can be found from Fig. 5(b) that the water absorption capability of every material grows with the increase of RH, and the trend of water absorption under different RH also matches the results observed by the hydration sorption curve. This is because the host carbon matrix plays the role of providing a support matrix and sorption surface for salt in the composite material. The higher the SSA and diversified porosity of the host matrix, the more conducive to the dispersing of water vapor and the uniform distribution of LiOH particles, which makes the hydration reaction of the composite material more complete, and leads to a huge enhancement in the hydration capability of the LiOH TES composite [41].

After selecting the best carbon matrix, the connection between the hydrated salt content and the hydration ability of the composite was investigated. It can be clearly observed from Fig. 6(a) that all Li/ZHCM2-x composites exhibit good hydration rate and water absorption capacity, in which Li/ZHCM2-40 presents the top hydration rate and water absorption. The explanation for this fact is that ZHCM2 with extremely high SSA and hierarchical microporous/mesoporous structure could offer an excellent support matrix and adsorption surface for LiOH, which can not only effectively alleviate the self-agglutination of LiOH, but also is more beneficial to the even scatter of salt hydrate, so that the interaction and reaction between lithium hydroxide and water become more thorough, and ultimately manifests as a huge enhancement in the hydration ability of Li/ZHCM2-x composites [42]. Note that when the salt proportion increases from 20% to 40%, the water absorption rate and capacity of Li/ZHCM2-x composites under the same RH also show a positive upward trend. For example, the equilibrium water absorption capacity of Li/ZHCM2-40 at 80% RH increases from 0.38 to $0.49 \text{ g}\cdot\text{g}^{-1}$. However, when the salt proportion increases from 40% to 50%, the water sorption rate and intensity exhibit the opposite trend. The inconsistency between the water uptake performance and the salt proportion of the Li/ZHCM2-x composites may be resulting from the excessively high salt proportion in Li/ZHCM2-50 aggravating the agglomeration of lithium hydroxide, which hampers the good scatter of hydrated salt on ZHCM2 and weakening the interaction and reaction with water, and finally leading to the decline of hydration ability [43]. The SEM results also confirm this conclusion (Fig. S2 in the ESM). Additionally, the water absorption capacities of Li/ZHCM2-x with different salt content under different RH were also explored. Figure 6(b) shows that the changing trend of the water absorption of each sample under various RH matches the observed results of the hydration adsorption isotherm, which further proves the changing trend between the salt content and the hydration capability of the Li/ZHCM2-x composites. Noticeably, the water absorption of

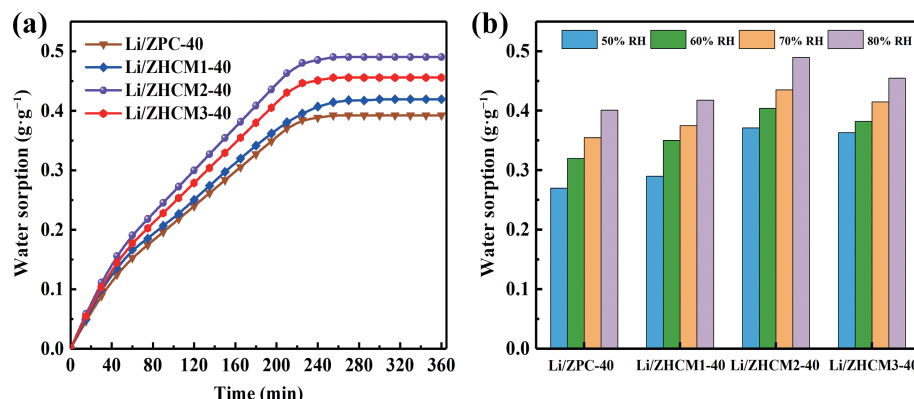


Figure 5 (a) Water sorption isotherms of LiOH TES materials with 40 wt.% salt at 30°C as well as 80% RH. (b) Water sorption capability of LiOH TES materials with 40 wt.% salts at 30°C with different RH.

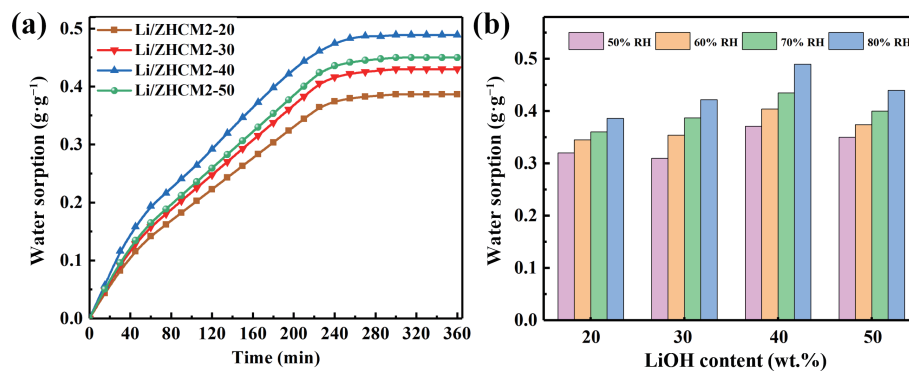


Figure 6 (a) Water absorption isotherms of Li/ZHCM2-20, Li/ZHCM2-30, Li/ZHCM2-40, and Li/ZHCM2-50 at 30 °C and 80% RH. (b) Equilibrium water absorption of Li/ZHCM2-20, Li/ZHCM2-30, Li/ZHCM2-40, and Li/ZHCM2-50 at 30 °C with various RH.

every composite at various RH has a positive correlation with RH. The above results on one hand prove the inseparable connection between RH, salt content and the hydration capability of the composite. On the other hand, it also confirms the superior hydration capability of the Li/ZHCM2-*x* composites and the indispensable and important role of ZHCM2 in the improvement of hydration performance.

In the light of the above results, it is clear that hydration temperature and RH are key parameters that play a vital role in hydration performance. Therefore, the effect of temperature and RH on the hydration ability of Li/ZHCM2 was evaluated. And Li/ZHCM2-40 was selected as a representative sample for the following test owing to its remarkable hydration performance. It can be found from Fig. 7(a) that when the temperature increases from 25 to 40 °C at the same RH, the hydration rate of the sample also becomes correspondingly faster and accompanied by a slight increase in the equilibrium water absorption, which shows that temperature only affects the time for the samples to reach the equilibrium state of hydration and has no significant effect on the equilibrium water absorption. On the other hand, Fig. 7(b) shows that when the RH is increased from 50% to 80% at a constant temperature, the hydration rate and equilibrium water absorption of Li/ZHCM2-40 both increase correspondingly. Notably, the Li/ZHCM2-*x* composites have no agglomeration and liquid leakage in the tests under all the above conditions, indicating that ZHCM2 as the host carbon matrix has played a very active role in overcoming the inherent problems of salt hydrate. It can be concluded that the Li/ZHCM2-*x* composite material, which exhibits excellent hydration performance under various conditions, has shown inestimable implementation value in the area of low-grade renewable energy storage.

3.3 Storage intensity of LiOH TES composites

For the purpose of clarifying the influence of the carbon matrix on

the energy storage strength of LiOH TES composites, the storage intensities of various LiOH TES composites with a range of carbon matrices were investigated. Figures 8(a)–(c) show that Li/ZPC-40 (1463.4 kJ·kg⁻¹) exhibits inferior storage intensity compared to the other two samples, which may be due to its relatively low SSA and insufficient mass transfer performance in the microporous structure based on BET results. After being activated by KOH, the heat storage performance of Li/ZHCM1-40 (1838.1 kJ·kg⁻¹) and Li/ZHCM3-40 (2185.2 kJ·kg⁻¹) shows a significant improvement ascribed to the growth of the corresponding SSA and hierarchical microporous/mesoporous structure. The reason for this phenomenon is that the larger the SSA and diversified porosity of the host carbon matrix that provides support matrix and sorption surface for salt, the more it contributes to the pervasion of water as well as the dispersion of LiOH particles, which enhances the hydration performance of the composites, and eventually greatly ameliorates the storage intensity of the LiOH TES composite materials [44]. It is also worth noting from Fig. 8(d) that the changing trend of the storage intensity of different samples is in step with the hydration capability, which verifies the close connection between the hydration capability and the heat storage intensity.

When the best carbon matrix was determined, the storage intensities of Li/ZHCM2-*x* with various salt proportions were also investigated. Figures 9(a)–9(d) display that all Li/ZHCM2 composites show great storage intensities. And the storage intensity of Li/ZHCM2-40 could reach the maximum of 2414.2 kJ·kg⁻¹, which is an increase of 134% compared with Li/ZHCM2-20. This is because ZHCM2 with ultrahigh SSA and hierarchical microporous/mesoporous structure provides an excellent support matrix and adsorption surface for LiOH, which not only be able to evidently weaken the self-agglutination of lithium hydroxide, but also has an active influence on its uniform dispersion, thereby improving the hydration performance of

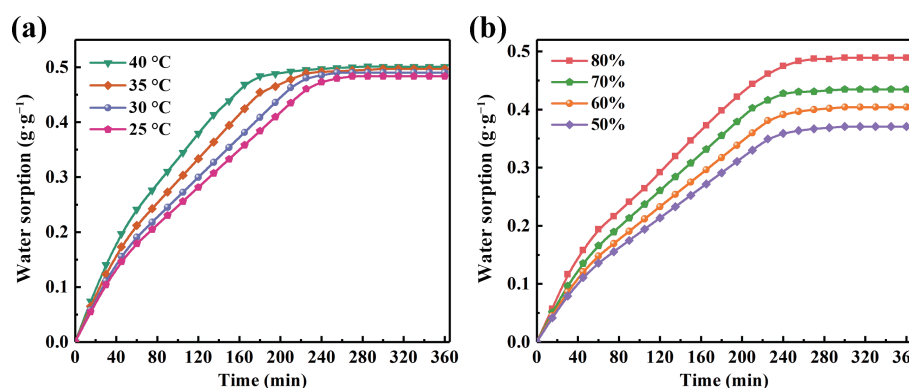


Figure 7 (a) Water sorption isotherms of Li/ZHCM2-40 at 80% RH with a range of hydration temperature. (b) Water sorption isotherms of Li/ZHCM2-40 at 30 °C with a range of RH.

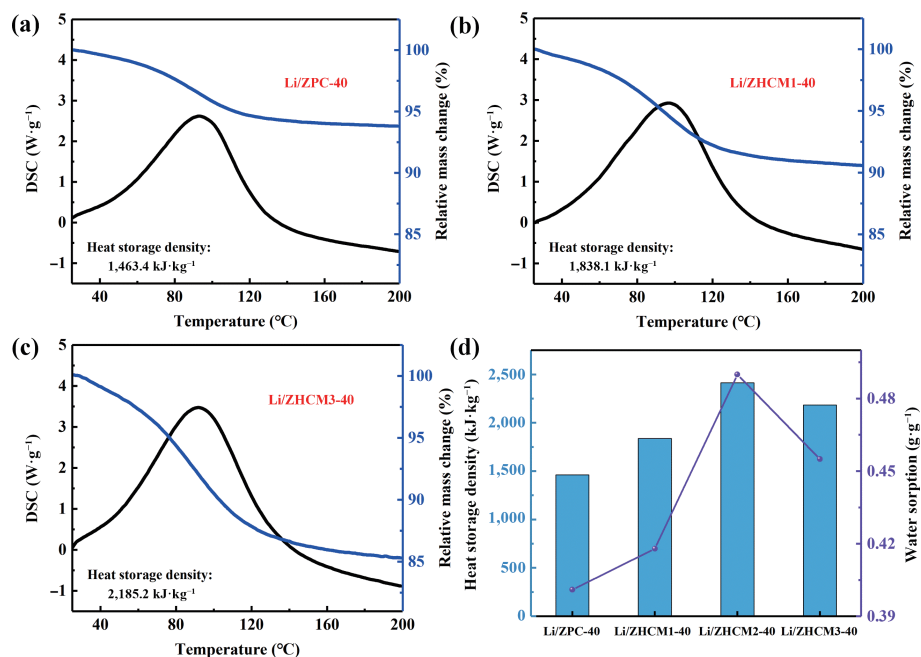


Figure 8 Synchronous thermal analysis (STA) curves of (a) Li/ZPC-40, (b) Li/ZHCM1-40, and (c) Li/ZHCM3-40. (d) The changing tide around storage intensity and water sorption of each LiOH TES composite.

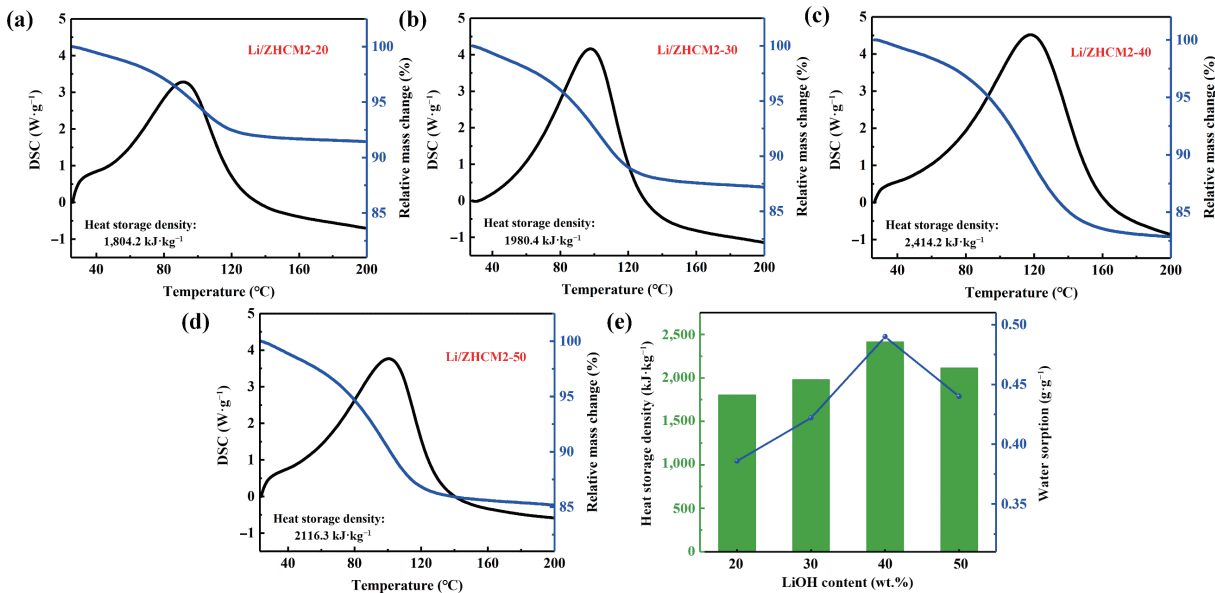


Figure 9 STA curves of ((a)–(d)) Li/ZHCM2-20, Li/ZHCM2-30, Li/ZHCM2-40, Li/ZHCM2-50. (f) The changing tide of storage intensity as well as water sorption with the proportion of Li/ZHCM2-x materials.

LiOH particles, and eventually causing a great increase in the storage intensity of Li/ZHCM2- x composites [44]. It is worth noting from Fig. 9(f) that when the mass fraction of hydrated salt increases from 20% to 40%, the storage intensity of the Li/ZHCM2 increases simultaneously. But when the mass fraction of hydrated salt increases from 40% to 50%, the storage intensity of the Li/ZHCM2-50 shows a downward trend. The storage intensity is not synchronized with the changing tide of the mass fraction of hydrated salt, which may be resulting from the excessively high salt proportion in Li/ZHCM2-50. This may aggravate the accumulation of LiOH in ZHCM2 and exhibit a negative influence on the even scatter of hydrated salt. Eventually, the water uptake capability of Li/ZHCM2-50 is weakened and manifests as the decrease in the storage intensity [43]. This judgment was also verified by SEM findings (Fig. S2 in the ESM). Furthermore, it should also be noted that the storage intensity of Li/ZHCM2 shows a changing trend in step with the hydration performance, which further confirms the fact that the hydration performance

has a direct and important influence on the storage intensity (Fig. 9(f)). It can be imagined that Li/ZHCM-40 with exceptional storage intensity as well as fabulous water sorption ability has demonstrated huge implementation value for effective low-grade renewable energy storage.

3.4 Cycle stability and heat transfer performance

Except for storage intensity and water sorption performance, cycle stability is also an important index for evaluating their practical implementation value. Therefore, Li/ZHCM2-40 was selected as a representative due to its excellent heat storage and hydration performance, and Li/ZHCM2-20 was used as a comparison to conduct cycle stability investigations through continuous hydration \leftrightarrow dehydration. From Fig. 10(a), it can be seen that the storage intensity of Li/ZHCM2-20 has decreased by 11.7%. By comparison, the storage intensity of Li/ZHCM2-40 (Fig. 10(b)) has only attenuated by 10.2%, which not only is a relatively lighter

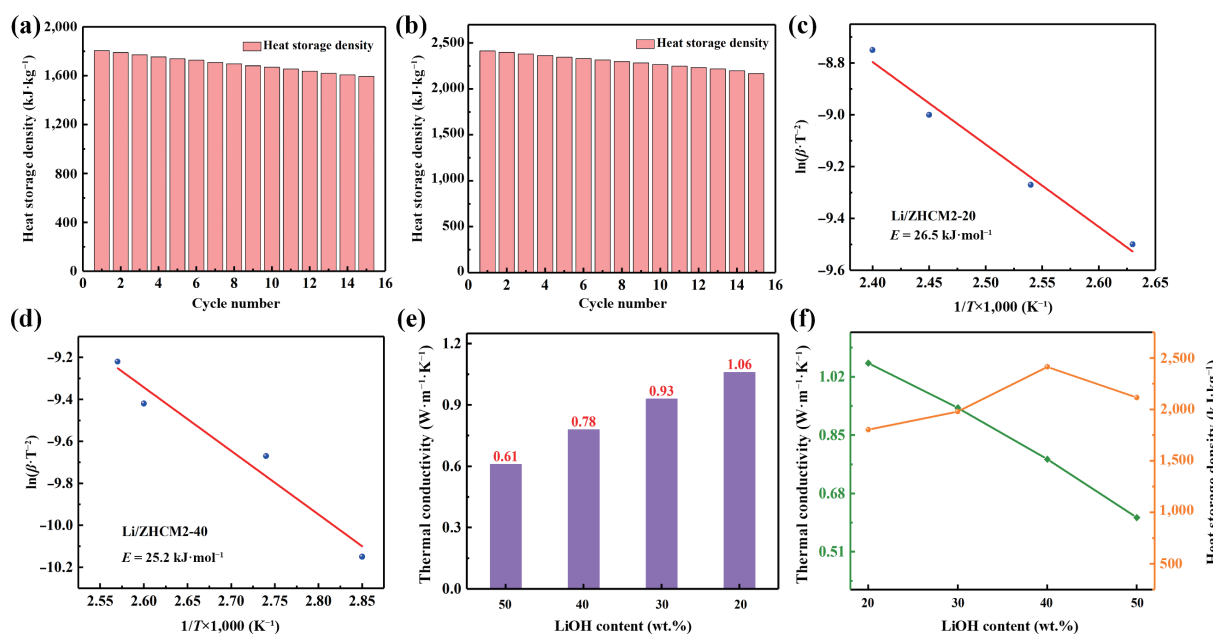


Figure 10 Cycle stability and activation energy of ((a) and (c)) Li/ZHCM2-20 and ((b) and (d)) Li/ZHCM2-40. (e) Thermal conductivity and (f) alteration of thermal conductivity with storage intensity of Li/ZHCM2-20, Li/ZHCM2-30, Li/ZHCM2-40 as well as Li/ZHCM2-50.

attenuation. Furthermore, the activation energy gap between the two samples also provides a further basis for explaining the above phenomenon. Figures 10(c) and 10(d) show that the activation energy required for Li/ZHCM2-40 ($25.2 \text{ kJ} \cdot \text{mol}^{-1}$) is smaller than that of Li/ZHCM2-20 ($26.5 \text{ kJ} \cdot \text{mol}^{-1}$), which indicates that it is less obstructed in the hydration process, thus resulting in better cycle stability of Li/ZHCM2-40.

Thermal conductivity is not only a key parameter representing the heat and mass transfer ability of heat storage materials, but also one of the important references for determining its application potential in actual reactor design. As shown in Fig. 10(e), owing to the prominent heat transfer capability of ZHCM2, the thermal conductivity of all Li/ZHCM2 composite materials has been significantly improved, and the Li/ZHCM2-20 presents the best heat transfer performance of $1.06 \text{ W} \cdot \text{m}^{-1} \cdot \text{K}^{-1}$. It should be noted from Fig. 10(f) that under the background that the thermal conductivity and storage intensity show a completely opposite trend with the change of the salt content, Li/ZHCM2-40, which is not only equipped with the best storage intensity, but also has a great thermal conductivity ($0.78 \text{ W} \cdot \text{m}^{-1} \cdot \text{K}^{-1}$), has become the optimum choice among all test samples after comprehensively weighing both heat transfer performance and storage intensity. In addition, the estimated cost of Li/ZHCM2-40 is about $\$10.3 \text{ kg}^{-1}$ according to the cost of $\text{Zn}(\text{CH}_3\text{COO})_2 \cdot 2\text{H}_2\text{O}$ ($\$3.16 \text{ kg}^{-1}$), 2-methylimidazole ($\26.2 kg^{-1}), KOH ($\$5.06 \text{ kg}^{-1}$) and $\text{LiOH} \cdot \text{H}_2\text{O}$ ($\$21.1 \text{ kg}^{-1}$), which also proves its practical application potential in actual space heating. On the other hand, it could be clearly observed from Table S2 in the ESM that in comparison to other hydrated salt-based TES materials, Li/ZHCM2-40 has exhibited great progress in various key heat storage parameters.

3.5 Heat transfer numerical simulation of the TES materials in micro heat storage reactor

For the purpose of obtaining a clearer picture of the heat transfer performance of TES materials, numerical simulations were carried out. As displayed in Fig. 11(a), the heat transfer numerical simulation is based on a micro heat storage reactor model, which is composed of two concentric cylinders. The central channel is a heat transfer fluid channel. On the outside of the central channel, TES materials are filled. In the heat storage stage, the saturated TES material is heated by high-temperature fluid, enabling the

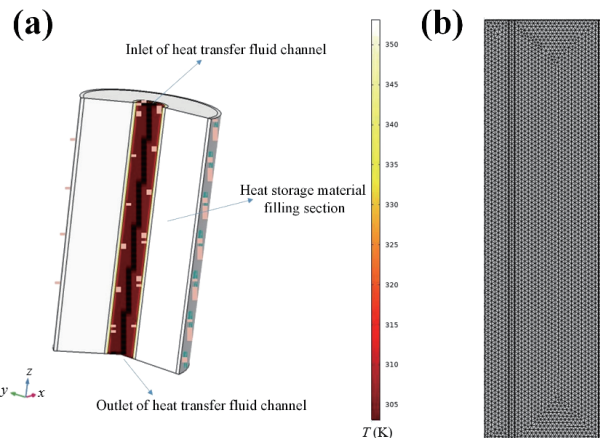


Figure 11 (a) 3D heat storage reactor model and (b) 2D mesh heat transfer model.

desorption and regeneration of the TES material. In the exothermic stage, the steam enters the TES material area for chemical reaction and releases heat. And the cold fluid is introduced into the central channel to replace the stored heat and complete the cycle. The initial conditions of the heat transfer simulation reaction were that during the adsorption reaction, nitrogen was used as the carrier gas to bring water vapor into the reactor along the direction of the fluid channel, and the inlet temperature of the reactor was 307 K , the gas flow rate was $50 \text{ mL} \cdot \text{min}^{-1}$, and the relative humidity was 80% . The current two-dimensional (2D) model was established in the finite element based solver COMSOL Multiphysics 5.4, as displayed in Fig. 11(b). The total number of grids was 7,428. The solid and fluid heat transfer interface, the Darcy law interface and the partial-differential equation interfaces were applied to establish the description of the above-mentioned model. And the model was solved through implicit, backward finite difference method in a transient solver with a maximum time step of 1 s.

Figure 12(a) shows the temperature distribution of pure lithium hydroxide TES material in micro reactor, and the temperature distribution is the change of temperature at different positions of longitudinal section of the three-dimensional (3D) reactor with the reaction time. The blue narrow area on the left is the

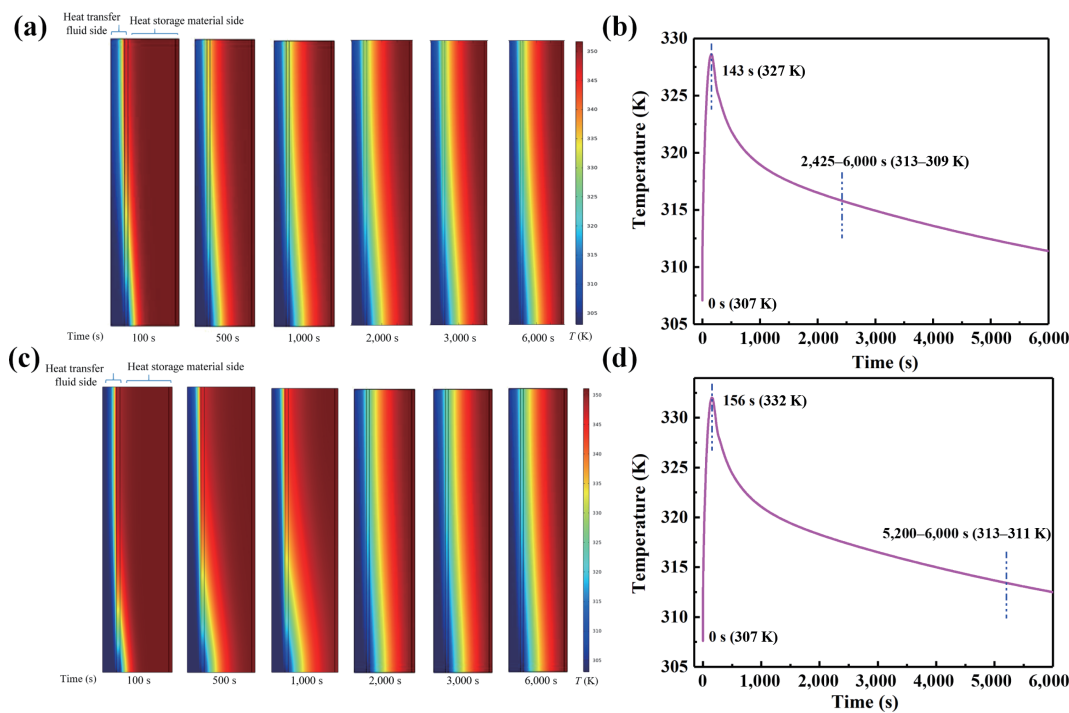


Figure 12 Microreactor temperature distribution and temperature change curve of heat transfer fluid outlet of ((a) and (b)) LiOH and ((c) and (d)) Li/ZHCM2-40.

temperature distribution of the heat transfer fluid channel, and the right is the temperature distribution of the TES material inside the reactor. When the reaction time reaches 100 s, the heat exchange between the heat transfer fluid and the TES material becomes obvious, and the temperature distribution also changes gradually. At 500 s, the temperature of the heat transfer fluid increases gradually, and the temperature of the TES material decreases. After 1,000 s, a significant temperature gradient appears inside the reactor and the cooling area of the TES material and the temperature of the heat transfer fluid also increase evidently. When the Li/ZHCM2-40 composite is filled into the reactor, the temperature distribution is similar to that of pure material (Fig. 12(c)). Figures 12(b) and 12(d) show the temperature change curve of heat transfer fluid outlet of pure lithium hydroxide and Li/ZHCM2-40 composite, respectively. It can be observed from Fig. 12(b) that the reaction continues to exotherm efficiently for 6,000 s, and the outlet temperature of the heat fluid rises rapidly between 0 and 143 s with the maximum temperature of 327 K. The temperature then slowly decreases, and the reactor outlet temperature is below 313 K after 2,425 s and finally drops to 309 K at 6,000 s. It is generally believed that when the temperature is lower than 313 K, the utilization rate of heat energy is very low, and it is necessary to stop the heat energy output and reactivate the TES material before it can continue to be used. The change of outlet temperature of heat transfer fluid filled with Li/ZHCM2-40 composite is similar to that of pure salt. Figure 12(d) displays that after 156 s of reaction, the outlet temperature of heat transfer fluid reaches 332 K, which is 5 K higher than the maximum temperature of pure salt. After 5,200 s, the outlet temperature of the Li/ZHCM2-40 composite-filled reactor is lower than 313 K, and the final temperature drops to 311 K. It is noteworthy that the time required for the outlet temperature of the Li/ZHCM2-40 composite-filled reactor to drop to 313 K is 2,775 s longer than that of the reactor filled with pure salt, indicating that the Li/ZHCM2-40 has a longer effective exothermic time. In addition, it cannot be ignored that when the TES material in the reactor reacts for a certain period of time, the outlet temperature of the reactor will drop significantly, which also known as the attenuation of the exothermic power of the reactor. This may be

due to the gradual agglomeration of the hydrated salt particles of the heat storage material during the reaction process, resulting in its surface being covered by agglomerates, which hinders the water vapor gas path, reduces the reaction efficiency, and ultimately reduces the exothermic power of the reactor. The appearance of such undesired phenomena further highlights the critical role and effectiveness of the host carbon matrix in the TES composite in assisting pure salts to weaken the agglomeration phenomenon and improve cycling stability. According to the above results, it can be confidently predicted that Li/ZHCM2-40 composite, which not only has distinguished storage intensity and water sorption capability, but also shows eminent cycle stability as well as heat transfer properties, will become an important bridge between the seasonal storage of renewable energy and the residential heating.

4 Conclusions

In summary, ZHCM2 has proven itself to be a distinguished and qualified host carbon matrix. More importantly, the Li/ZHCM2-40, which exerts the advantageous properties of lithium hydroxide and the ZIF-8 derived host carbon matrix while minimizing their respective shortcomings, has also been demonstrated to be a prominent hydrated salt-based TES material. On the basis of ensuring the various structural advantages of ZPC, ZHCM2 could further make up for the regret of monotonous porosity through appropriate chemical activation, while the corresponding SSA has also achieved great progress. In addition, as the host carbon matrix of TES composites, ZHCM2 with hierarchical microporous/mesoporous structure and extremely high SSA offers an excellent support matrix and adsorption surface for hydrated salt, which can not only effectively alleviate a series of remaining shortcomings of LiOH, but also is beneficial to the great improvement in the storage performance of the Li/ZHCM2. In fact, the fabricated Li/ZHCM2-40 shows a prominent storage intensity up to 2414.2 kJ·kg⁻¹ and a low charging temperature, while also having exceptional hydration performance arising from the favorable adsorption surface and appropriate water vapor diffusion aisles supported by ZHCM2. Furthermore, the storage intensity of Li/ZHCM2-40 attenuates only 10.2% after 15 repeated

charge-discharge processes, which demonstrates its eminent cycle stability. And because of the excellent heat transfer performance of the carbon matrix, the Li/ZHCM2 also shows superior thermal conductivity. Besides, the numerical simulation results further prove its great heat transfer performance. This new LiOH TES composite not only opens a valuable approach for effective low grade thermochemical energy storage as well as utilization, but also provides new possibilities for the further implementation of MOF derived carbon matrix in the future.

Acknowledgements

The authors appreciate the support from the Key-Area Research and Development Program of Guangdong Province (No. 2020B0202010004), the National Natural Science Foundation of China (No. 52071192), and the Key Research Program of Frontier Sciences, Chinese Academy of Sciences (CAS) (No. QYZDY-SSW-JSC038).

Electronic Supplementary Material: Supplementary material (reagents, characterization and heat transfer numerical simulation description; SEM images; textural characteristics and comparison table of Li/ZHCM2-40 composite and other salt hydrates) is available in the online version of this article at <https://doi.org/10.1007/s12274-022-4415-2>.

References

- Carrillo, A. J.; González-Aguilar, J.; Romero, M.; Coronado, J. M. Solar energy on demand: A review on high temperature thermochemical heat storage systems and materials. *Chem. Rev.* **2019**, *119*, 4777–4816.
- Li, Y. T.; Li, M. T.; Xu, Z. B.; Meng, Z. H.; Wu, Q. P. Dehydration kinetics and thermodynamics of $ZrO(NO_3)_2$ -doped $Ca(OH)_2$ for chemical heat storage. *Chem. Eng. J.* **2020**, *399*, 125841.
- Koohi-Fayegh, S.; Rosen, M. A. A review of energy storage types, applications and recent developments. *J. Energy Storage* **2020**, *27*, 101047.
- Yu, Z. P.; Feng, D. L.; Feng, Y. H.; Zhang, X. X. Thermal conductivity and energy storage capacity enhancement and bottleneck of shape-stabilized phase change composites with graphene foam and carbon nanotubes. *Compos. A Appl. Sci. Manuf.* **2022**, *152*, 106703.
- Biesuz, M.; Valentini, F.; Bortolotti, M.; Zambotti, A.; Cestari, F.; Bruni, A.; Sglavo, V. M.; Sorarù, G. D.; Dorigato, A.; Pegoretti, A. Biogenic architectures for green, cheap, and efficient thermal energy storage and management. *Renew. Energy* **2021**, *178*, 96–107.
- Cabeza, L. F.; De Gracia, A.; Zsembinszki, G.; Borri, E. Perspectives on thermal energy storage research. *Energy* **2021**, *231*, 120943.
- Qi, G. Q.; Yang, J.; Bao, R. Y.; Xia, D. Y.; Cao, M.; Yang, W.; Yang, M. B.; Wei, D. C. Hierarchical graphene foam-based phase change materials with enhanced thermal conductivity and shape stability for efficient solar-to-thermal energy conversion and storage. *Nano Res.* **2017**, *10*, 802–813.
- Li, A. J.; Xu, W. Z.; Chen, R.; Liu, Y. C.; Li, W. Fabrication of zeolitic imidazolate frameworks on layered double hydroxide nanosheets to improve the fire safety of epoxy resin. *Compos. A Appl. Sci. Manuf.* **2018**, *112*, 558–571.
- Peng, J. J.; Tao, J.; Liu, Z. J.; Yang, Y. H.; Yu, L.; Zhang, M.; Wang, F.; Ding, Y. Ultra-stable and high capacity flexible lithium-ion batteries based on bimetallic MOFs derivatives aiming for wearable electronic devices. *Chem. Eng. J.* **2021**, *417*, 129200.
- Gulbalkan, H. C.; Haslak, Z. P.; Altintas, C.; Uzun, A.; Keskin, S. Assessing CH_4/N_2 separation potential of MOFs, COFs, IL/MOF, MOF/Polymer, and COF/Polymer composites. *Chem. Eng. J.* **2022**, *428*, 131239.
- Gordeeva, L. G.; Tu, Y. D.; Pan, Q. W.; Palash, M. L.; Saha, B. B.; Aristov, Y. I.; Wang, R. Z. Metal-organic frameworks for energy conversion and water harvesting: A bridge between thermal engineering and material science. *Nano Energy* **2021**, *84*, 105946.
- Chen, Y. Z.; Zhang, R.; Jiao, L.; Jiang, H. L. Metal-organic framework-derived porous materials for catalysis. *Coord. Chem. Rev.* **2018**, *362*, 1–23.
- Wang, J.; Wang, Y. L.; Hu, H. B.; Yang, Q. P.; Cai, J. J. From metal-organic frameworks to porous carbon materials: Recent progress and prospects from energy and environmental perspectives. *Nanoscale* **2020**, *12*, 4238–4268.
- DeCoste, J. B.; Peterson, G. W. Metal-organic frameworks for air purification of toxic chemicals. *Chem. Rev.* **2014**, *114*, 5695–5727.
- Zhu, L. N.; Meng, L. J.; Shi, J. Q.; Li, J. H.; Zhang, X. S.; Feng, M. B. Metal-organic frameworks/carbon-based materials for environmental remediation: A state-of-the-art mini-review. *J. Environ. Manag.* **2019**, *232*, 964–977.
- Chung, D. Y.; Lee, K. J.; Yu, S. H.; Kim, M.; Lee, S. Y.; Kim, O. H.; Park, H. J.; Sung, Y. E. Alveoli-inspired facile transport structure of N-doped porous carbon for electrochemical energy applications. *Adv. Energy Mater.* **2015**, *5*, 1401309.
- Bai, F. H.; Xia, Y. D.; Chen, B. L.; Su, H. Q.; Zhu, Y. Q. Preparation and carbon dioxide uptake capacity of N-doped porous carbon materials derived from direct carbonization of zeolitic imidazolate framework. *Carbon* **2014**, *79*, 213–226.
- Zhang, Y. N.; Dong, H. H.; Wang, R. Z.; Feng, P. H. Air humidity assisted sorption thermal battery governed by reaction wave model. *Energy Stor. Mater.* **2020**, *27*, 9–16.
- Li, W.; Klemeš, J. J.; Wang, Q. W.; Zeng, M. Salt hydrate-based gas-solid thermochemical energy storage: Current progress, challenges, and perspectives. *Renew. Sust. Energy Rev.* **2022**, *154*, 111846.
- Jiang, F.; Ge, Z. W.; Ling, X.; Cang, D. Q.; Zhang, L. L.; Ding, Y. L. Improved thermophysical properties of shape-stabilized $NaNO_3$ using a modified diatomite-based porous ceramic for solar thermal energy storage. *Renew. Energy* **2021**, *179*, 327–338.
- Donkers, P. A. J.; Sögütoglu, L. C.; Huinink, H. P.; Fischer, H. R.; Adan, O. C. G. A review of salt hydrates for seasonal heat storage in domestic applications. *Appl. Energy* **2017**, *199*, 45–68.
- Alva, G.; Lin, Y. X.; Fang, G. Y. An overview of thermal energy storage systems. *Energy* **2018**, *144*, 341–378.
- Zhang, Y. N.; Wang, R. Z.; Li, T. X. Thermochemical characterizations of high-stable activated alumina/LiCl composites with multistage sorption process for thermal storage. *Energy* **2018**, *156*, 240–249.
- Zhao, Y. J.; Wang, R. Z.; Zhang, Y. N.; Yu, N. Development of $SrBr_2$ composite sorbents for a sorption thermal energy storage system to store low-temperature heat. *Energy* **2016**, *115*, 129–139.
- Solé, A.; Martorell, I.; Cabeza, L. F. State of the art on gas-solid thermochemical energy storage systems and reactors for building applications. *Renew. Sust. Energy Rev.* **2015**, *47*, 386–398.
- Yan, T.; Wang, R. Z.; Li, T. X.; Wang, L. W.; Fred, I. T. A review of promising candidate reactions for chemical heat storage. *Renew. Sust. Energy Rev.* **2015**, *43*, 13–31.
- Kubota, M.; Matsumoto, S.; Matsuda, H.; Huang, H. Y.; He, Z. H.; Yang, X. X. Chemical heat storage with $LiOH/LiOH \cdot H_2O$ reaction for low-temperature heat below 373 K. *Adv. Mater. Res.* **2014**, *953–954*, 757–760.
- Kubota, M.; Matsumoto, S.; Matsuda, H. Enhancement of hydration rate of $LiOH$ by combining with mesoporous carbon for low-temperature chemical heat storage. *Appl. Therm. Eng.* **2019**, *150*, 858–863.
- Li, W.; Klemeš, J. J.; Wang, Q. W.; Zeng, M. Development and characteristics analysis of salt-hydrate based composite sorbent for low-grade thermochemical energy storage. *Renew. Energy* **2020**, *157*, 920–940.
- Li, W.; Klemeš, J. J.; Wang, Q. W.; Zeng, M. Characterisation and sorption behaviour of $LiOH-LiCl@EG$ composite sorbents for thermochemical energy storage with controllable thermal upgradeability. *Chem. Eng. J.* **2021**, *421*, 129586.
- Wang, R. T.; Jin, D. D.; Zhang, Y. B.; Wang, S. J.; Lang, J. W.; Yan, X. B.; Zhang, L. Engineering metal organic framework derived 3D nanostructures for high performance hybrid supercapacitors. *J.*

- Mater. Chem. A* **2017**, *5*, 292–302.
- [32] Qie, L.; Chen, W. M.; Xu, H. H.; Xiong, X. Q.; Jiang, Y.; Zou, F.; Hu, X. L.; Xin, Y.; Zhang, Z. L.; Huang, Y. H. Synthesis of functionalized 3D hierarchical porous carbon for high-performance supercapacitors. *Energy Environ. Sci.* **2013**, *6*, 2497–2504.
- [33] Zheng, X. Y.; Lv, W.; Tao, Y.; Shao, J. J.; Zhang, C.; Liu, D. H.; Luo, J. Y.; Wang, D. W.; Yang, Q. H. Oriented and interlinked porous carbon nanosheets with an extraordinary capacitive performance. *Chem. Mater.* **2014**, *26*, 6896–6903.
- [34] Zhong, H. X.; Wang, J.; Zhang, Y. W.; Xu, W. L.; Xing, W.; Xu, D.; Zhang, Y. F.; Zhang, X. B. ZIF-8 derived graphene-based nitrogen-doped porous carbon sheets as highly efficient and durable oxygen reduction electrocatalysts. *Angew. Chem., Int. Ed.* **2014**, *53*, 14235–14239.
- [35] Deng, X. Y.; Li, J. J.; Zhu, S.; Ma, L. Y.; Zhao, N. Q. Boosting the capacitive storage performance of MOF-derived carbon frameworks via structural modulation for supercapacitors. *Energy Stor. Mater.* **2019**, *23*, 491–498.
- [36] Li, Y. G.; Zhou, W.; Wang, H. L.; Xie, L. M.; Liang, Y. Y.; Wei, F.; Idrobo, J. C.; Pennycook, S. J.; Dai, H. J. An oxygen reduction electrocatalyst based on carbon nanotube-graphene complexes. *Nat. Nanotechnol.* **2012**, *7*, 394–400.
- [37] Sevilla, M.; Mokaya, R. Energy storage applications of activated carbons: Supercapacitors and hydrogen storage. *Energy Environ. Sci.* **2014**, *7*, 1250–1280.
- [38] Li, Z.; Xu, Z. W.; Tan, X. H.; Wang, H. L.; Holt, C. M. B.; Stephenson, T.; Olsen, B. C.; Mitlin, D. Mesoporous nitrogen-rich carbons derived from protein for ultra-high capacity battery anodes and supercapacitors. *Energy Environ. Sci.* **2013**, *6*, 871–878.
- [39] Feng, L. X.; Wang, K.; Zhang, X.; Sun, X. Z.; Li, C.; Ge, X. B.; Ma, Y. W. Flexible solid-state supercapacitors with enhanced performance from hierarchically graphene nanocomposite electrodes and ionic liquid incorporated gel polymer electrolyte. *Adv. Funct. Mater.* **2018**, *28*, 1704463.
- [40] Shen, J. M.; Li, Y.; Wang, C. H.; Luo, R.; Li, J. S.; Sun, X. Y.; Shen, J. Y.; Han, W. Q.; Wang, L. J. Hollow ZIFs-derived nanoporous carbon for efficient capacitive deionization. *Electrochim. Acta* **2018**, *273*, 34–42.
- [41] Clark, R. J.; Mehrabadi, A.; Farid, M. State of the art on salt hydrate thermochemical energy storage systems for use in building applications. *J. Energy Stor.* **2020**, *27*, 101145.
- [42] Li, S. J.; Huang, H. Y.; Li, J.; Kobayashi, N.; Osaka, Y.; He, Z. H.; Yuan, H. R. The effect of 3D carbon nanoadditives on lithium hydroxide monohydrate based composite materials for highly efficient low temperature thermochemical heat storage. *RSC Adv.* **2018**, *8*, 8199–8208.
- [43] Wang, Q.; Xie, Y. Y.; Ding, B.; Yu, G. L.; Ye, F.; Xu, C. Structure and hydration state characterizations of MgSO₄-zeolite 13x composite materials for long-term thermochemical heat storage. *Sol. Energy Mater. Sol. Cells* **2019**, *200*, 110047.
- [44] Li, S. J.; Huang, H. Y.; Yang, X. X.; Bai, Y.; Li, J.; Kobayashi, N.; Kubota, M. Hydrophilic substance assisted low temperature LiOH·H₂O based composite thermochemical materials for thermal energy storage. *Appl. Therm. Eng.* **2018**, *128*, 706–711.